Inorganic Chemistry

Article

pubs.acs.org/IC

Unique Ligand-Radical Character of an Activated Cobalt Salen Catalyst That Is Generated by Aerobic Oxidation of a Cobalt(II) Salen Complex

Takuya Kurahashi and Hiroshi Fujii*

Institute for Molecular Science & Okazaki Institute for Integrative Bioscience, National Institutes of Natural Sciences, Myodaiji, Okazaki, Aichi 444-8787, Japan

Supporting Information

ABSTRACT: The Co(salen)(X) complex, where salen is chiral *N*,*N*′-bis(3,5-di-*tert*-butylsalicylidene)-1,2-cyclohexanediamine and X is an external axial ligand, has been widely utilized as a versatile catalyst. The Co(salen)(X) complex is a stable solid that has been conventionally described as a Co^{III}(salen)(X) complex. Recent theoretical calculations raised a new proposal that the Co(salen)(H_2O)(SbF_6) complex contains appreciable contribution from a Co^{II}(salen$^{\bullet+}$) electronic structure (Kochem, A.; Kanso, H.; Baptiste, B.; Arora, H.; Philouze, C.; Jarjayes, O.; Vezin, H.; Luneau, D.; Orio, M.; Thomas, F. *Inorg. Chem.* **2012**, *51*, 10557−10571), while other theoretical calculations for Co(salen)(Cl) indicated a triplet Co^{III}(salen) electronic structure (Kemper, S.; Hrobárik, P.; Kaupp, M.; Schlörer, N. E. *J. Am. Chem. Soc.* **2009**, *131*, 4172−4173). However, there have been no experimental data to evaluate these theoretical proposals. We herein report key experimental data on the electronic structure of the Co(salen)(X) complex (X = $CF_3SO_3^-$, SbF_6^-, and *p*-$MeC_6H_4SO_3^-$). The X-ray crystallography shows that Co(salen)(OTf) has a square-planar N_2O_2 equatorial coordination sphere with OTf as an elongated external axial ligand. Magnetic susceptibility data indicate that Co(salen)(OTf) complexes belong to the S = 1 spin system. ^{1}H NMR measurements provide convincing evidence for the Co^{II}(salen$^{\bullet+}$)(X) character, which is estimated to be about 40% in addition to 60% Co^{III}(salen)(X) character. The CH_2Cl_2 solution of Co(salen)(X) shows an intense near-IR absorption, which is assigned as overlapped transitions from a ligand-to-metal charge transfer in Co^{III}(salen)(X) and a ligand-to-ligand charge transfer in Co^{II}(salen$^{\bullet+}$)(X). The present experimental study establishes that the electronic structure of Co(salen)(X) contains both Co^{II}(salen$^{\bullet+}$)(X) and Co^{III}(salen)(X) character.

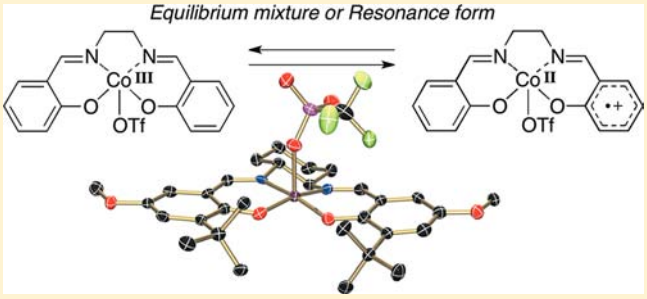

INTRODUCTION

A cobalt salen complex has gained considerable attention over the past decade, since Jacobsen discovered that a cobalt complex with Jacobsen's chiral salen ligand, *N*,*N*′-bis(3,5-di-*tert*-butylsalicylidene)-1,2-cyclohexanediamine, is an excellent catalyst for the hydrolytic kinetic resolution of terminal epoxides.[1,2] It has also been demonstrated that the same cobalt salen complex and its derivatives are highly effective in other reactions,[3] such as CO_2/epoxides polymerization.[4,5] The key is that the catalyst is not a well-studied cobalt(II) salen complex[6] but an activated form that is prepared by aerobic oxidation of a cobalt(II) salen complex. The activated cobalt salen catalyst is readily synthesized by the addition of protic acid to the solution of a cobalt(II) salen complex under aerobic conditions and could be isolated as a stable solid that has a Co(salen)(X) composition, where X is derived from a counterion of protic acid. The most commonly used axial ligand X is AcO^- ($CH_3CO_2^-$) as in the original report by Jacobsen,[2a] but other counterions are also employed such as Cl^-,[3g] TsO^- (*p*-$MeC_6H_4SO_3^-$),[2f] SbF_6^-,[3b,j] and TfO^- ($CF_3SO_3^-$)[3m] for various catalytic reactions.

Conventionally, the Co(salen)(X) complex is described simply as a cobalt(III) salen complex, even in mechanistic studies that have been reported to investigate the excellent catalytic activity of Co(salen)(X).[7] This is because the Co(salen)(X) complexes, dissolved in strongly coordinating dimethyl sulfoxide, exhibit ^{1}H NMR signals within a diamagnetic region, which is consistent with a low-spin, diamagnetic Co^{III} d^6. In most of the other solvents, Co(salen)(X) complexes display paramagnetic behavior, but little is known about the details of the paramagnetic species, which might be responsible for catalytic reactions. Kaupp, Schlörer, and co-workers investigated a paramagnetic Co(salen)(Cl) complex in a noncoordinating CD_2Cl_2 solvent by analyzing a formidably complicated paramagnetic ^{1}H NMR spectrum, in combination with density functional theory (DFT) calculations.[7e] They showed that the complication of the NMR spectrum comes from large differences between paramagnetic shifts on two different halves of the salen ligand, which they ascribed as arising from a twisted solution conformation and a

Received: December 6, 2012
Published: March 21, 2013

triplet cobalt(III) center. Van Doorslaer and co-workers investigated the oxidation process of Co^{II}(salen) under aerobic conditions in the presence of acetic acid.[7h] By using continuous-wave and pulsed electron paramagnetic resonance (EPR) and resonance Raman techniques, they detected a cobalt(III) ligand-radical species as an EPR-active minor species, with the majority species being EPR-silent, most probably Co^{III}(salen)(OAc). Very recently, during the preparation of this manuscript, Thomas and co-workers reported another DFT result that indicates that, in the Co(salen)-$(H_2O)(SbF_6)$ complex, 30% of the total spin density is distributed over the salen ligand, while the remaining 70% is localized on the cobalt center.[8] Their calculations also suggested that the spin density on cobalt is slightly increased from 70−75% upon replacement of $(H_2O)(SbF_6)$ by AcO. Their new proposal is seemingly contradictory to the previous DFT result for triplet Co^{III}(salen)(Cl) by Kaupp et al.[7e] However, there have been no experimental data to evaluate these theoretical proposals.

We herein report molecular and electronic structures of the Co(salen)(X) complex (X = AcO^-, TsO^-, SbF_6^-, and TfO^-), as a part of our studies on metal salen complexes.[9] Although the formal oxidation state of cobalt is III+ for Co(salen)(X) bearing dianionic salen and monoanionic X ligands, the experimental oxidation state of cobalt could be different physically or spectroscopically because a redox-active salen ligand could be oxidized to a salen ligand radical. It is well established that nickel and copper salen complexes in the formal oxidation state of III+ bearing a weakly coordinating ligand such as SbF_6^- are salen ligand-radical (salen$^{\bullet+}$) complexes with low-valent nickel(II) or copper(II) ions.[10−12] In contrast, it is generally accepted that iron and manganese salen complexes are iron(III) or manganese(III) with a nonradical salen ligand.[9g] The cobalt ion is positioned in the middle of manganese/iron and nickel/copper in the periodic table, and thus the electronic structure of Co(salen)(X) deserves careful investigation. The present study reveals that the Co(salen)(X) complex shows spectroscopic properties consistent with the Co^{II}(salen$^{\bullet+}$) electronic structure in the case of X = TsO^-, SbF_6^-, and TfO^-, contrary to the previous assignment as a cobalt(III) complex. However, the Co(salen)(X) complex also exhibits a near-IR (NIR) absorption that could be assigned as a ligand-to-metal charge-transfer transition, as expected for the Co^{III}(salen) electronic structure. The present experimental study establishes that the electronic structure of Co(salen)(X) contains both Co^{II}(salen$^{\bullet+}$)(X) and Co^{III}(salen)(X) character.

RESULTS AND DISCUSSION

Preparation and Electrochemical Properties of Co(salen)(X). In addition to symmetrical salen ligands, we prepare unsymmetrical salen ligands bearing two phenolates with different redox potentials (Chart 1), which was previously utilized as a powerful tool to unambiguously determine ligand-to-ligand charge-transfer transitions in salen ligand-radical complexes.[9f] A Co^{II}(salen) complex was oxidized aerobically under biphasic CH_2Cl_2−TfOH/H_2O conditions, which gave a pure product that has a Co(salen)(OTf) composition.

Cyclic voltammetry measurements were carried out at 233 K in CH_2Cl_2 containing 0.1 M Bu_4NOTf (Figure S1, Supporting Information, SI), and the electrochemical parameters referenced versus the ferrocenium/ferrocene couple (Fc^+/Fc) are summarized in Table 1. The formal Co^{II}/Co^{III} redox cycle in Co(L-*t*-Bu)(OTf) appears at −0.10 V versus Fc^+/Fc, which is significantly lower than the redox potential that is required to generate a salen ligand radical (L-*t*-Bu$^{\bullet+}$) coordinated to nickel(II) and copper(II) (0.37 and 0.45 V, respectively).[10h,11a] This is consistent with the observation that the Co(salen)-(OTf) complex is readily synthesized by aerobic oxidation of Co^{II}(salen). The $E_{1/2}$ value for the formal Co^{II}/Co^{III} cycle is increased in the order MeO (−0.11 V) < *t*-Bu (−0.10 V) < Cl (−0.08 V) as a substituent on the salen ligand (Figure S8, SI). However, the increase of the $E_{1/2}$ value upon exchange of the substituent is very small compared with that of the Ni^{II}(salen) and Mn^{III}(salen)(OTf) complexes, which generate nickel(II) or manganese(III) ligand-radical species; $E_{1/2}$ for Ni^{II}(salen), MeO (0.21 V) < *t*-Bu (0.36 V) < Cl (0.49 V) and $E_{1/2}$ for Mn^{III}(salen)(OTf), MeO (0.46 V) < *t*-Bu (0.70 V) < Cl (0.86 V).[9f]

Chart 1. Symmetrical and Unsymmetrical Salen Ligands and Their Abbreviations

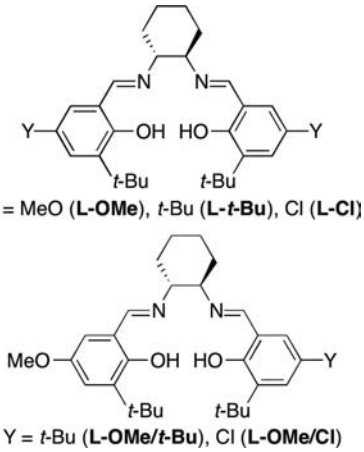

Table 1. Electrochemical Parameters (Formally Co^{III}/Co^{II}) Measured in CH_2Cl_2 Containing 0.1 M Bu_4NOTf at 233 K under an Argon Atmosphere[a]

	E_c (V)	E_a (V)	$E_{1/2}$ (V)
Co(L-OMe)(OTf)	−0.166	−0.046	−0.106
Co(L-*t*-Bu)(OTf)	−0.188	−0.015	−0.101
Co(L-Cl)(OTf)	−0.180	+0.023	−0.078
Co(L-OMe/*t*-Bu)(OTf)	−0.162	−0.055	−0.108
Co(L-OMe/Cl)(OTf)	−0.150	−0.030	−0.090

[a] E_c is a cathodic reduction peak potential and E_a is an anodic oxidation peak potential. $E_{1/2}$ values are calculated as averaged values of E_a and E_c. Potentials are referenced versus the Fc^+/Fc couple. Potentials are determined with cyclic voltammetry (Figure S1, SI).

X-ray Crystal Structure. We attempted to crystallize all of the Co(salen)(OTf) complexes and obtained a crystal of Co(L-OMe)(OTf) suitable for X-ray crystallography. Figure 1 shows the X-ray crystal structure of Co(L-OMe)(OTf). Crystallographic data are summarized in Table S1, SI. The asymmetric cell contains two molecules, **a** and **b**, and the packing diagram is shown in Figure S2, SI. Table 2 lists the structural parameters of **a** and **b**, in comparison with the starting Co^{II}(L-OMe) complex.[8] Co(L-OMe)(OTf) possesses a square-planar N_2O_2 equatorial coordination sphere with OTf as an elongated external axial ligand (Co−OTf distance = 2.134 and 2.124 Å for **a** and **b**, respectively). We carefully compared the structural parameters of the phenolate rings between Co(L-OMe)(OTf) and Co^{II}(L-OMe), in order to consider whether the Co(L-

dx.doi.org/10.1021/ic302677f | Inorg. Chem. 2013, 52, 3908−3919

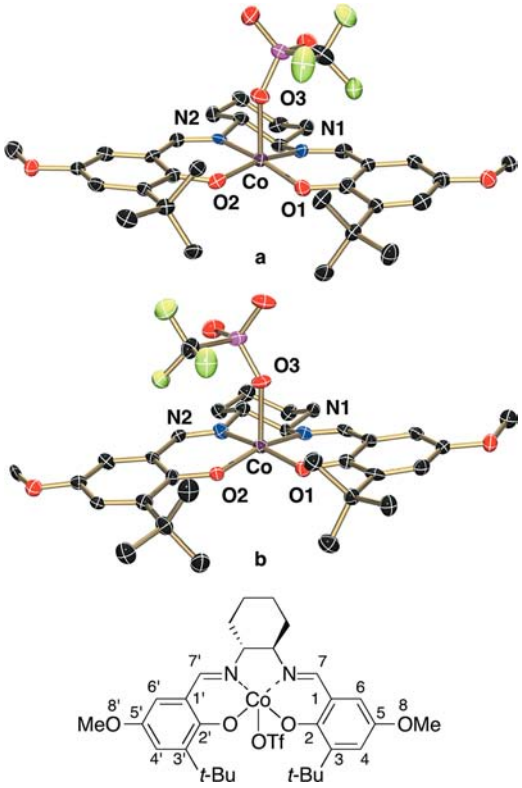

Figure 1. X-ray crystal structure of Co(L-OMe)(OTf). The asymmetric cell contains two molecules, which are designated as **a** and **b**. The structural parameters of **a** and **b** are shown in Table 2. Thermal ellipsoids represent the 50% probability surfaces. Hydrogen atoms are omitted for the sake of clarity.

Table 2. Structural Parameters for Co(L-OMe)(OTf) in Comparison with Co^{II}(L-OMe)[a]

distance (Å)	a	b	Co^{II}(L-OMe)
Co−O1	1.842(5)	1.861(5)	1.846
Co−O2	1.856(5)	1.830(5)	1.846
Co−O3	2.134(6)	2.124(5)	
Co−N1	1.871(6)	1.872(6)	1.857
Co−N2	1.868(6)	1.880(6)	1.857
O1−C2	1.314(9)	1.301(9)	1.311
O2−C2′	1.319(9)	1.338(9)	1.311
C5−O8	1.390(10)	1.379(10)	1.383
C5′−O8′	1.368(10)	1.347(9)	1.383
N1−C7	1.300(10)	1.283(10)	1.296
N2−C7′	1.306(10)	1.299(9)	1.296
C1−C2	1.425(9)	1.440(8)	1.416
C2−C3	1.444(9)	1.455(9)	1.439
C3−C4	1.356(11)	1.353(10)	1.378
C4−C5	1.407(10)	1.410(9)	1.405
C5−C6	1.371(9)	1.372(10)	1.361
C1−C6	1.406(11)	1.409(11)	1.418
C1′−C2′	1.422(8)	1.419(9)	1.416
C2′−C3′	1.443(9)	1.440(9)	1.439
C3′−C4′	1.385(10)	1.395(11)	1.378
C4′−C5′	1.411(9)	1.417(9)	1.405
C5′−C6′	1.358(10)	1.374(9)	1.361
C1′−C6′	1.425(11)	1.407(10)	1.418

[a]The structural parameters of Co^{II}(L-OMe) are shown as averaged values of the left and right moieties from two molecules in the asymmetric cell. The data are adopted from ref 8.

OMe)(OTf) complex exhibits ligand-radical character or not (Figure S3, SI). Thomas and co-workers have already reported that the salen ligand radicals (L-$OMe^{\bullet+}$) with Cu^{II} and Ni^{II} show the formation of a quinoid-like structure, in which the C1−C6 and C3−C4 bonds of the phenolate ring are shortened by 0.02−0.05 Å, with the other bonds being similar or longer compared with those of the parent salen complexes (0−0.05 Å).[12] The C3−C4 bond of Co(L-OMe)(OTf) is slightly shortened from that of Co^{II}(L-OMe) by 0.02 Å, which might arise from the formation of the ligand radical, but the other bonds of the phenolate rings are not altered within experimental error. The quinoid-like deformation is not so evident for Co(L-OMe)(OTf), indicating that the Co(L-OMe)(OTf) complex has significant Co^{III}(L-OMe)(OTf) character compared with the Co^{II}(L-$OMe^{\bullet+}$)(OTf) character. NMR measurements indeed show that the Co^{III}(L-OMe)(OTf) and Co^{II}(L-$OMe^{\bullet+}$)(OTf) character is 60 and 40%, respectively (vide infra).

L-Edge X-ray Absorption Spectroscopy. Figure 2 shows a Co L-edge X-ray absorption spectrum of Co(L-*t*-Bu)(OTf),

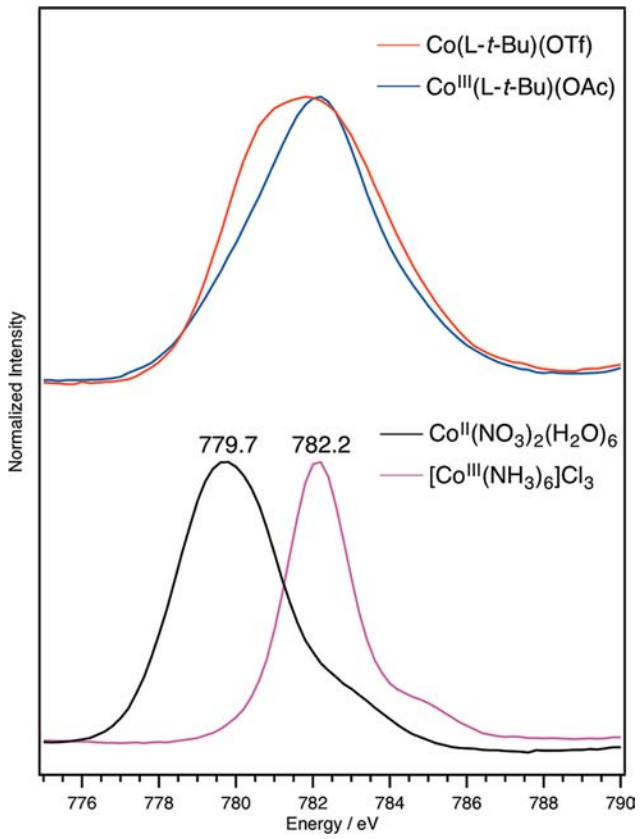

Figure 2. Co L_3-edge X-ray absorption spectra of Co(L-*t*-Bu)(OTf) (red line) and diamagnetic Co^{III}(L-*t*-Bu)(OAc) (blue line), in comparison with $Co^{II}(NO_3)_2(H_2O)_6$ (black line) and $[Co^{III}(NH_3)_6]Cl_3$ (purple line) as reference compounds.

which is compared with the spectrum of Co^{III}(L-*t*-Bu)(OAc) bearing a diamagnetic Co^{III} d^6 center as clearly indicated by ^{1}H NMR (Figure S4, SI). Figure 2 only shows the L_3-edge region of the Co L-edge X-ray absorption spectra because the L_3-edge shows more significant changes than the L_2-edge in the present case (Figures S5 and S6, SI). Each spectrum is a sum of five scans, and no appreciable change is observed for the first and final scans after X-ray irradiation for 1 h (Figure S7, SI). The

dx.doi.org/10.1021/ic302677f | Inorg. Chem. 2013, 52, 3908−3919

Co L-edge X-ray absorption spectra of Co(L-*t*-Bu)(OTf) (red line) and Co^{III}(L-*t*-Bu)(OAc) (blue line) are slightly different. The Co(L-*t*-Bu)(OTf) complex apparently shows an additional absorption in the lower-energy region, compared with the diamagnetic Co^{III}(L-*t*-Bu)(OAc) complex. The same spectral feature is observed for Co(L-OMe)(OTf) and Co(L-Cl)(OTf), irrespective of the substituents on the salen ligand. Figure 2 also shows Co L-edge X-ray absorption spectra of $Co^{II}(NO_3)_2(H_2O)_6$ and $[Co^{III}(NH_3)_6]Cl_3$ as reference compounds. The Co L-edge X-ray absorption of cobalt(II) in $Co^{II}(NO_3)_2(H_2O)_6$ appears at 779.7 eV, which is lower than the absorption of cobalt(III) in $[Co^{III}(NH_3)_6]Cl_3$ at 782.2 eV. Then, the additional absorption at the lower-energy region for Co(L-*t*-Bu)(OTf) seemingly suggests that Co(L-*t*-Bu)(OTf) has cobalt(II) character in addition to cobalt(III) character. However, the absorption spectral change between Co(L-*t*-Bu)(OTf) and Co^{III}(L-*t*-Bu)(OAc) could be alternatively interpreted as excitations to empty d orbitals of different energy rather than excitations from the cobalt ion of different oxidation states.[13]

Magnetic Properties of the Co(salen)(OTf) Complexes. Figure 3 shows the temperature dependence of magnetic moments of solid samples of Co^{II}(L-OMe) and Co(L-OMe)(OTf). The μ_{eff} versus T plots were fitted by using the *julX* program, which solves the following spin Hamiltonian:

$$H = g\beta H(S_1 + S_2) - JS_1 \cdot S_2 + D(S_z^2 - 1/3S^2) + E(S_x^2 - S_y^2) \quad (1)$$

where S_1 and S_2 are the spins on the cobalt and salen ligand radical and D and E are the zero-field-splitting parameters. J is the exchange coupling constant between spins of the cobalt and salen ligand radical. The second term vanishes when spins exist only on the cobalt center. Co^{II}(L-OMe) shows magnetic moments of 2.1−2.2 μ_B in the range 20−320 K, which is consistent with Co^{II} d^7 species in a square-planar geometry ($S = {}^1/_2$).[14] In contrast, Co(L-OMe)(OTf) shows a magnetic moment of 2.9−3.0 μ_B in the range 50−320 K, which is close to the spin-only value for the $S = 1$ system (2.828 μ_B). The $S = 1$ spin system corresponds to triplet Co^{III} d^6, and the drop of the magnetic moment below 50 K could be fitted by a large zero-field splitting ($|D| = 36$ cm^{-1}; red line in Figure 3). In addition, the $S = 1$ spin system can also arise from the salen ligand radical ($S = {}^1/_2$) coupled with Co^{III} d^7 ($S = {}^1/_2$), and the drop of the magnetic moment below 50 K could be fitted by weak antiferromagnetic coupling ($J = -4.5$ cm^{-1}) between the salen ligand radical and cobalt(II) ion (blue line in Figure 3). Thus, both Co^{III}(salen)(X) and Co^{II}(salen$^{\bullet+}$)(X) electronic structures could account for the observed magnetic susceptibility data.

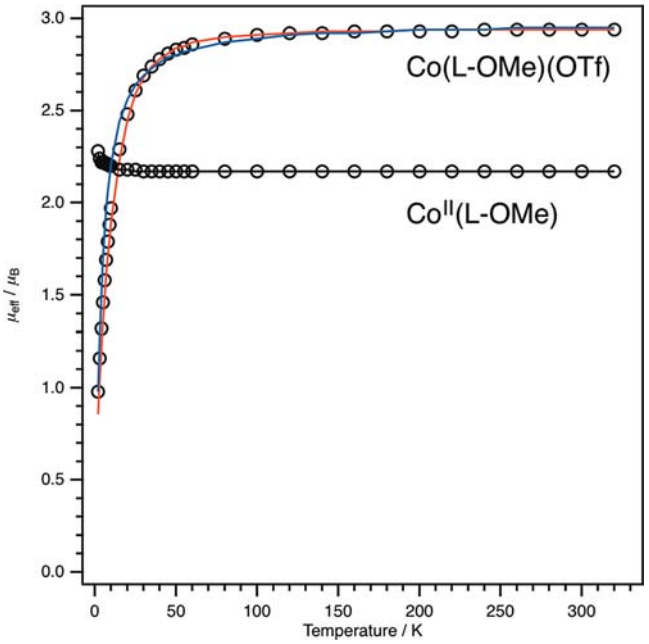

Figure 3. Temperature dependence of the magnetic moment (μ_{eff}) of polycrystalline samples of Co^{II}(L-OMe) and Co(L-OMe)(OTf) in an applied field of 1 kOe. The solid lines represent one of possible fits with parameters for Co^{II}(L-OMe) (black line) of $S = {}^1/_2$, $g = 2.5$, $\chi_{TIP} = 350 \times 10^{-6}$ emu, and $\theta = 0.18$ K, for Co^{III}(L-OMe)(OTf) (red line) of $S = 1$, $[D] = 36$ cm^{-1}, $E/D = 0.3$, $g = 2.08$, and $\chi_{TIP} = 250 \times 10^{-6}$ emu, and those for Co^{II}(L-OMe$^{\bullet+}$)(OTf) (blue line) as follows: the salen ligand ($S = {}^1/_2$) that is involved in weak antiferromagnetic coupling with cobalt(II) ($S = {}^1/_2$); $J = -4.5$ cm^{-1}; $D = 0.5$ cm^{-1}; $g = 2.8$ (Co^{II}) and 2.0 (L-OMe$^{\bullet+}$); $\chi_{TIP} = 250 \times 10^{-6}$ emu; $\theta = -3.0$ K.

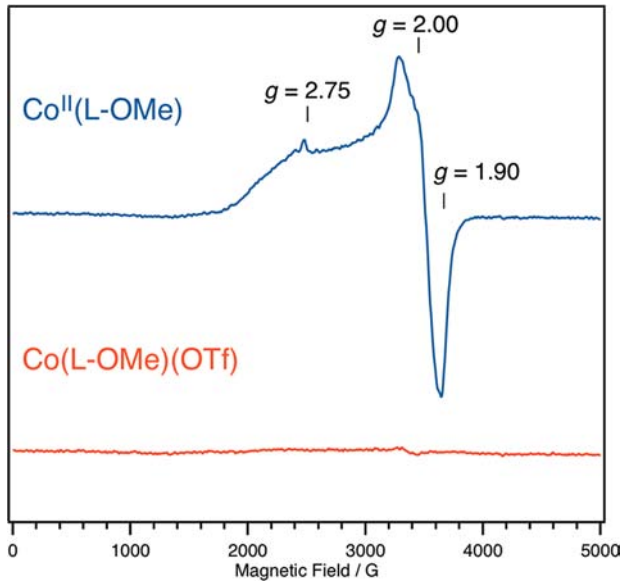

Figure 4. X-band EPR spectra of 2 mM frozen solutions of Co^{II}(L-OMe) (blue line) and Co(L-OMe)(OTf) (red line). Conditions: temperature, 4 K; solvent, frozen 30% toluene−CH_2Cl_2; microwave frequency, 9.65 GHz; microwave power, 0.5 mW; modulation amplitude, 7G; time constant, 163.84 ms; conversion time, 163.84 ms. The g values are determined by the simulation using *EasySpin* (Figure S12, SI).

As shown in Figure 4, the $S = {}^1/_2$ Co^{II}(L-OMe) complex exhibits EPR signals at $g = 2.75$, 2.00, and 1.90. These signals are assigned as arising from unpaired electrons in the dπ (d_{xz} or d_{yz}) orbital. The $(d\pi)^1$ ground state for Co^{II}(salen) in a noncoordinating solvent is also consistent with ^{1}H NMR spectra (vide infra). Upon aerobic oxidation, the intense EPR signal observed for Co^{II}(L-OMe) completely disappears (Figure 4), which clearly indicates that aerobic oxidation of Co^{II}(L-OMe) accompanies one-electron oxidation, generating a species in the formal oxidation state of III+. Magnetic susceptibility and EPR data of other complexes show that aerobic oxidation of Co^{II}(salen) in the presence of TfOH

dx.doi.org/10.1021/ic302677f | *Inorg. Chem.* 2013, 52, 3908−3919

Table 3. ^{1}H or ^{2}H NMR Shifts of Co^{II}(salen) Complexes in CD_2Cl_2 (CH_2Cl_2) and Pyridine-d_5 (Pyridine)[a]

	phenolate/ppm	azomethine/ppm	3-*tert*-butyl/ ppm	5-substituent/ppm	cyclohexane/ppm
Co^{II}(L-OMe)					
in CD_2Cl_2	12.8, 12.9	−51.0	15.2	4.0 (methoxy)	7.0, 17.2, 18.3, 107.3
in pyridine-d_5	14.5, 17.0	not determined	8.0	4.4 (methoxy)	6.0, 7.6, 10.5, 39.9, 43.1
Co^{II}(L-*t*-Bu)					
in CD_2Cl_2	10.9, 13.7	−55.6	16.4	−0.5 (*tert*-butyl)	7.9, 18.4, 19.5, 20.5, 112.9
in pyridine-d_5	15.4, 17.7	50.8	7.9	1.7 (*tert*-butyl)	6.4, 7.4, 10.4, 37.6, 57.1
Co^{II}(L-Cl)					
in CD_2Cl_2	10.1, 14.7	−57.9	17.9		8.6, 19.3, 20.9, 22.4, 111.3
in pyridine-d_5	17.2, 20.7	not determined	8.7		8.0, 9.4, 11.6, 38.1, 117.9
Co^{II}(L-OMe/*t*-Bu)	11.2, 12.4 13.0, 13.6	−56.1, −50.2	15.7	−0.4 (*tert*-butyl), 3.8 (methoxy)	7.4, 17.7, 18.8, 19.5
Co^{II}(L-OMe/Cl)	11.0, 12.1 12.8, 14.9	−55.8, −52.9	16.4	3.8 (methoxy)	7.6, 7.9, 18.2, 19.5, 20.5, 103.9, 119.7

[a] ^{1}H and ^{2}H NMR spectra are shown in Figures S13, S15, and S19−S21 (SI).

Table 4. ^{1}H or ^{2}H NMR Shifts of Co(salen)(OTf) Complexes in CD_2Cl_2 or CH_2Cl_2[a]

	phenolate/ppm	azomethine/ ppm	3-*tert*-butyl/ ppm	5-substituent/ppm	cyclohexane/ppm
Co(L-OMe)(OTf)	27.9, 51.6	−123	0.9	30.9 (methoxy)	−16.7, −1.7, 4.7, 8.0, 205
Co(L-*t*-Bu)(OTf)	31.6, 57.5	−144	1.1	8.0 (*tert*-butyl)	−17.9, −0.1, 4.6, 8.5, 185
Co(L-Cl)(OTf)	34.7, 58.3	−153	1.2		−19.0, 0.3, 4.6, 8.6, 174
Co(L-OMe/*t*-Bu)(OTf)	29.5, 30.0, 53.2, 54.7	−145, −120	0.8, 1.2	7.6 (*tert*-butyl) 33.3 (methoxy)	−17.2, −17.0, −2.1, 0.2, 4.5, 4.7, 8.9, 175, 217
Co(L-OMe/Cl)(OTf)	29.9, 32.6, 52.1, 53.8	−143, −123	0.5, 1.7	39.4 (methoxy)	−17.8, −16.8, −3.1, 1.4, 4.5, 4.8, 6.9, 9.7, 145, 244
Co(L-*t*-Bu)(SbF_6)	31.7, 59.2	−150	1.0	8.5 (*tert*-butyl)	−18.8, −0.3, 4.7, 9.0, 188
Co(L-*t*-Bu)(OTs)	28.6, 52.0	not observed	1.0	6.9 (*tert*-butyl)	−17.5, −0.2, 4.2, 7.6

[a] ^{1}H and ^{2}H NMR spectra are shown in Figures 6 and 7 and S14, S16, and S22 (SI).

generates the same Co(salen)(OTf) complexes, irrespective of the substituent on the salen ligand (Figures S9−S11, SI).

NMR Study. In order to investigate the electronic structure of Co(salen)(X) in more detail, we measured ^{1}H NMR spectra of Co^{II}(salen) and Co(salen)(X) (X = TsO^-, SbF_6^-, and TfO^-) in CD_2Cl_2. The chemical shifts and assignments of ^{1}H NMR signals are summarized in Tables 3 and 4. The ^{1}H NMR signals of Co^{II}(L-*t*-Bu) and Co(L-*t*-Bu)(OTf) were assigned by ^{2}H NMR of cobalt salen complexes that are selectively deuterated at phenolate, *tert*-butyl, and azomethine groups (Figures S13 and S14, SI). ^{1}H NMR spectra of Co^{II}(L-OMe)/Co^{II}(L-Cl) and Co^{III}(L-OMe)(OTf)/Co^{III}(L-Cl)(OTf) show shift patterns similar to those of Co^{II}(L-*t*-Bu)/Co(L-*t*-Bu)(OTf), indicative of an identical electronic structure (Figures S15 and S16, SI). These data enabled us to assign ^{1}H NMR signals of Co^{II}(L-OMe)/Co^{II}(L-Cl) and Co^{III}(L-OMe)(OTf)/Co^{III}(L-Cl)(OTf), as well as the *tert*-butyl groups at the 3/3′ and 5/5′ positions in Co^{II}(L-*t*-Bu)/Co(L-*t*-Bu)(OTf). The ^{1}H and ^{2}H NMR signals of paramagnetic Co^{II}(salen) and Co(salen)(OTf) show normal Curie's law behavior, which shows a linear correlation of the chemical shift with $1/T$ from 193 to 298 K with intercepts in the diamagnetic region (Figures S17 and S18, SI). As shown in Table 3, ^{1}H NMR spectra of Co^{II}(salen) in CD_2Cl_2 and pyridine-d_5 substantially differ with the azomethine ^{2}H NMR signals at −55.6 and 50.8 ppm in CH_2Cl_2 and pyridine, respectively. This clearly indicates that the Co^{II}(salen) complexes adopt electronic structures with unpaired electrons in dπ (d_{xz} or d_{yz}) and d_{z^2} orbitals in dichloromethane and pyridine, respectively, which induces different paramagnetic shifts via through bond (contact shift) and through space (dipolar shift). This change arises from the coordination of pyridine to the cobalt(II) center.[6b]

Figure 5 shows ^{1}H NMR spectra of Co^{II}(L-OMe) and Co(L-OMe)(OTf) in CD_2Cl_2 at 298 K. ^{1}H NMR signals of the phenolate protons at 4/4′ and 6/6′ positions for Co(L-OMe)(OTf) are observed at 51.6 and 27.9 ppm, respectively, which are largely shifted from 12.8 and 12.9 ppm for Co^{II}(L-OMe). Large downfield shifts of the phenolate protons are observed for all of the Co(salen)(OTf) complexes (Table 4). In addition, the ^{1}H NMR signal of the MeO group also shows a significantly large downfield shift from 4.0 ppm in Co^{II}(L-OMe) to 30.9 ppm in Co(L-OMe)(OTf). Such a large downfield shift cannot be explained by a spin-transfer mechanism from the S = 1 cobalt(III) paramagnetic center because unpaired electrons in the cobalt dπ or d_{z^2} orbital induce almost no paramagnetic shift for the MeO signal, as is clearly seen from the ^{1}H NMR spectra of Co^{II}(salen) with a $(d\pi)^1$ or $(d_{z^2})^1$ ground-state electronic configuration (Table 3). Therefore, ^{1}H and ^{2}H NMR spectra clearly indicate that the electronic structure of Co(salen)(OTf) contains a contribution from the Co^{II}(salen$^{\bullet+}$)(OTf) state, in which a π-radical spin on the salen ligand is a predominant factor for the paramagnetic shift for the MeO group as well as the phenolate protons.

In order to evaluate the contribution from Co^{II}(salen$^{\bullet+}$)-(OTf) in a quantitative manner, we calculated a paramagnetic shift of the MeO signal that is induced by a salen ligand π-radical spin. Equation 2 correlates a paramagnetic NMR contact shift (δ_{con}) with a proton hyperfine coupling constant (a^H in joules).[15,16] The a^H in joules is derived from the experimental a^H in tesla by eq 3.

$$\delta_{con} = a^H \frac{g\mu_B}{4\hbar\gamma_H k_B T} \quad (2)$$

dx.doi.org/10.1021/ic302677f | Inorg. Chem. 2013, 52, 3908−3919

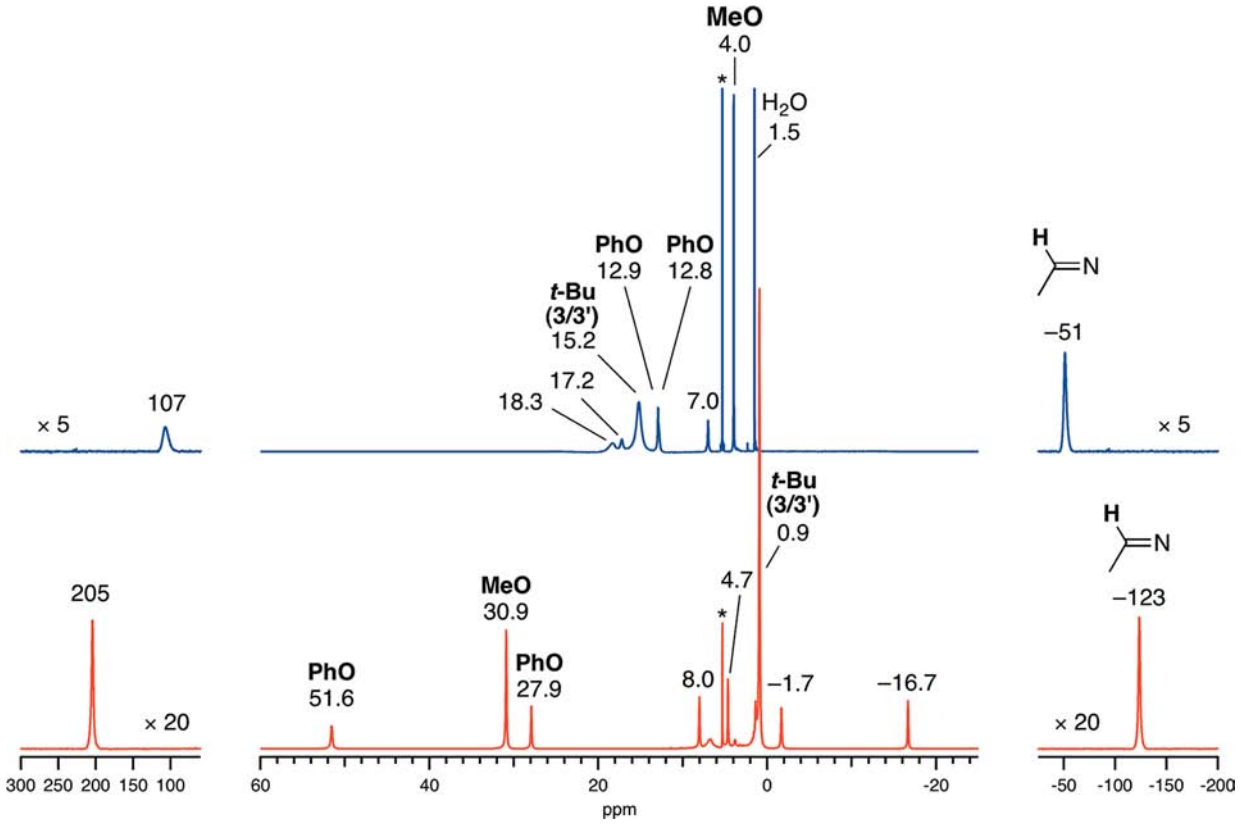

Figure 5. ^{1}H NMR spectra of a 20 mM solution of Co^{II}(L-OMe) (blue line) and Co(L-OMe)(OTf) (red line) in CD_2Cl_2 at 298 K. The signals denoted with asterisks come from residual $CHDCl_2$ and are referenced to 5.32 ppm. The *tert*-butyl, phenolate, and azomethine protons are assigned by comparing the ^{1}H and ^{2}H NMR spectra of Co^{II}(L-*t*-Bu), Co(L-*t*-Bu)(OTf), and selectively deuterated complexes (Figures S13−S16, SI) and are denoted with "*t*-Bu" and "PhO".

$$a^{H}\,(J) = g\mu_B a^{H}\,(T) \qquad (3)$$

where g is the g factor (2.002), μ_B is the Bohr magneton (9.274×10^{-24} J T^{-1}), $\hbar$ is the reduced Planck constant (1.054×10^{-34} J s), γ_H is the proton gyromagnetic ratio (2.675×10^{8} s^{-1} T^{-1}), k_B is the Bolzmann constant (1.381×10^{-23} J K^{-1}), and T is the absolute temperature (298 K in the present case). The a^H value for the MeO group, which has not been reported for L-OMe$^{\bullet+}$ with any metal, is estimated to be in the range from 0.172 to 0.218 mT from phenoxyl radical species in similar systems.[17] The calculation predicts a 64−81 ppm downfield shift for the MeO signal, as the averaged value between the phenolate and phenoxyl radical moieties, in the Co^{II}(L-OMe$^{\bullet+}$)(OTf) complex at 298 K. The observed change upon one-electron oxidation from Co^{II}(L-OMe) to Co(L-OMe)(OTf) is a 27 ppm downfield shift at 298 K. This indicates that the percentage of the Co^{II}(L-OMe$^{\bullet+}$)(OTf) electronic structure is 33−42%, with the remaining 67−58% being the Co^{III}(L-OMe)(OTf) electronic structure. This result is nicely consistent with the DFT calculation reported by Thomas et al., which indicates that 30% of the total spin density in Co(L-OMe)(SbF_6) is distributed over the aromatic ring, with the remaining 70% being localized on the cobalt.[8] The ^{1}H NMR shifts of the other Co(salen)(OTf) are close to those of Co(L-OMe)(OTf), and thus the percentage of Co^{II}(salen$^{\bullet+}$)(OTf) is estimated to be almost the same, irrespective of the substituent (MeO, *t*-Bu, and Cl) on the salen ligand. Because ^{1}H and ^{2}H NMR signals for the Co^{III}(salen)(OTf) and Co^{II}(salen$^{\bullet+}$)(OTf) electronic structures are not separated, these two structures exchange much faster than the NMR time scale. Moreover, the phenolate and phenoxyl radical moieties in Co^{II}(salen$^{\bullet+}$)(OTf) also exchange much faster than the NMR time scale because of rapid intramolecular electron transfer. Then, it should be noted that the Co(salen)(OTf) complexes show averaged NMR shifts among these species.

In order to obtain additional evidence for the ligand-radical character, we measured ^{1}H NMR spectra of unsymmetrical Co(L-OMe/*t*-Bu)(OTf) and Co(L-OMe/Cl)(OTf) (Figure 6). Co(L-OMe/*t*-Bu)(OTf) and Co(L-OMe/Cl)(OTf) show separate signals for the left and right sides of the salen ligands, which are close to those of symmetrical Co(L-OMe)(OTf). This observation indicates that a radical spin on the salen ligand is distributed almost comparably, but not evenly, over the left and right salicylidene rings in nonsymmetrical Co(L-OMe/*t*-Bu)(OTf) and Co(L-OMe/Cl)(OTf) (Scheme 1) because of the very small difference in the formal Co^{II}/Co^{III} redox cycle for Co(L-OMe)(OTf), Co(L-*t*-Bu)(OTf), and Co(L-Cl)(OTf), as shown in Table 1. Quite interestingly, the MeO signal on one phenolate (30.9 ppm) is significantly shifted downfield upon exchange of the substituent on the other phenolate to *t*-Bu (33.3 ppm) and Cl (39.4 ppm), indicating that the percentage of radical character on the phenolate bearing a MeO group is increased in the order MeO < *t*-Bu < Cl as a substituent on the other phenolate (Scheme 1). This order is consistent with the difference of the redox potentials of Co(salen)(OTf), as shown in Table 1. Such shifts of the MeO signal are not observed for other salen complexes with no ligand-radical character.[9g] The ^{1}H NMR spectra of unsymmetrical Co(L-OMe/*t*-Bu)(OTf) and Co(L-OMe/Cl)(OTf) thus provide additional strong

dx.doi.org/10.1021/ic302677f | *Inorg. Chem.* 2013, 52, 3908−3919

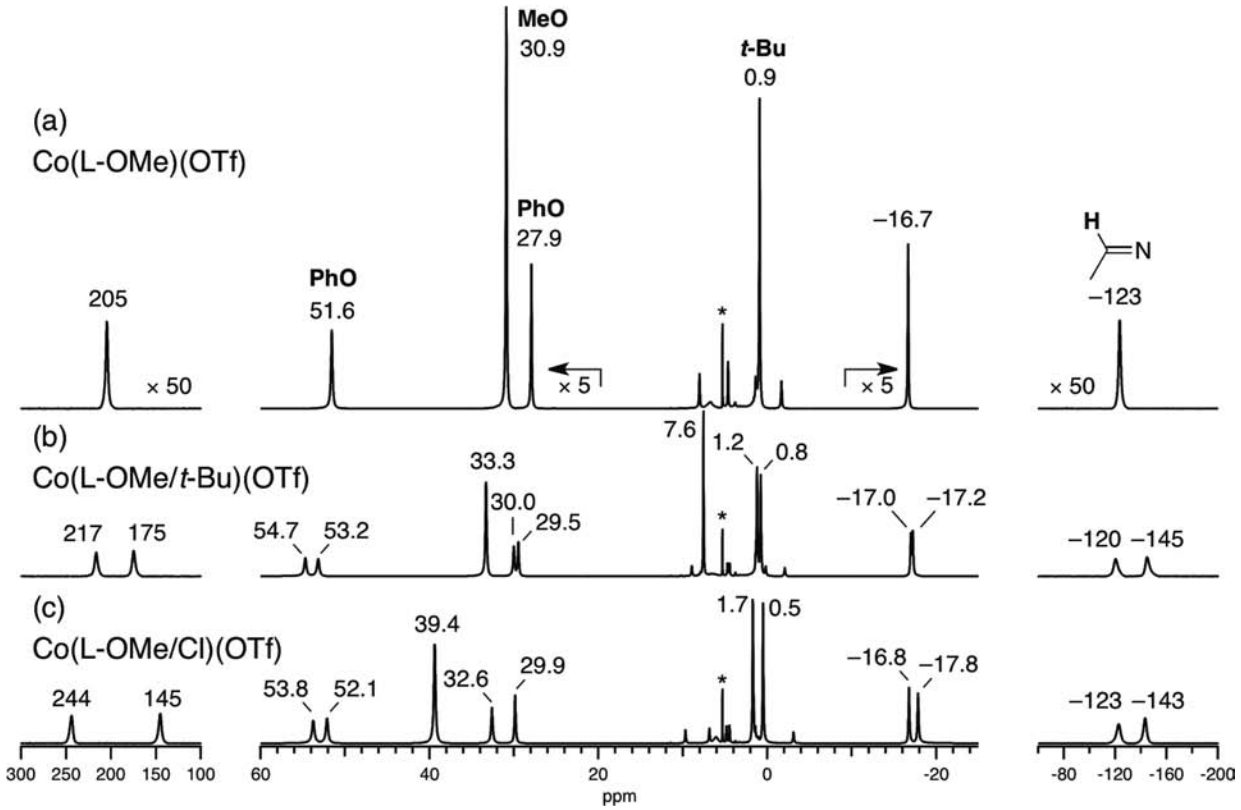

Figure 6. ^{1}H NMR spectra of 20 mM solution of (a) Co(L-OMe)(OTf), (b) Co(L-OMe/*t*-Bu)(OTf), and (c) Co(L-OMe/Cl)(OTf) in CD_2Cl_2 at 298 K. The signals designated with asterisks come from residual $CHDCl_2$ and are referenced to 5.32 ppm. The signals designated with "MeO", "*t*-Bu", and "PhO" arise from the MeO, *tert*-butyl, and phenolate protons, respectively.

Scheme 1. Additional Evidence for Ligand-Radical Character

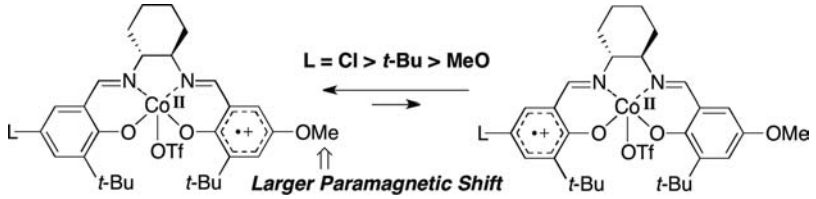

evidence for the ligand-radical character of the Co(salen)(OTf) complex.

We then investigated axial-ligand effects and prepared Co(L-*t*-Bu)(H_2O)(SbF_6)[8] and Co(L-*t*-Bu)(OTs). ^{1}H NMR spectra of Co(L-*t*-Bu)(H_2O)(SbF_6) and Co(L-*t*-Bu)(OTs) show the same shift patterns as that of Co(L-*t*-Bu)(OTf) (Table 4), indicative of the identical electronic structure irrespective of the TfO^-, SbF_6^-, and TsO^- axial ligands. The magnitudes of the paramagnetic shifts slightly increase in the order TsO^- < TfO^- < SbF_6^-, which suggests that the ligand-radical character might slightly increase in this order, possibly because of lower binding affinity to the cobalt center. The Co(L-*t*-Bu)(OAc) complex adopts a diamagnetic Co^{III} d^6 electronic configuration, which arises not only from the higher binding affinity of AcO^- but also from the six-coordinate structure induced by a chelating AcO^- ligand.[7j] The coordination of Cl^- as an axial ligand gave a mixture of paramagnetic and diamagnetic species in CD_2Cl_2, as reported by Kaupp and Schlörer.[7e] The ^{1}H NMR shift pattern of a paramagnetic species from Co(L-*t*-Bu)(Cl), which is assigned as a triplet cobalt(III) complex by means of DFT calculations, is strikingly different from that of the present Co(L-*t*-Bu)(X) (X = TfO^-, SbF_6^-, and TsO^-).

Spectroscopic Properties. The Co(salen)(OTf) complexes show an intense, broad absorption around 1000 nm (Figure 7a), which is not observed for the Co^{II}(salen) complexes (Figure S23, SI). This spectroscopic feature was already mentioned in the recent paper by Thomas et al.[8] We investigated the origin of this NIR absorption in more detail. The characteristic NIR absorptions in Co(salen)(OTf) are also observed in the solid state at nearly the same wavelength (Figure S24, SI), indicating that the electronic structures of Co(salen)(OTf) are not altered between the solid state and the CH_2Cl_2 solution. Because the Co(salen)(OTf) complexes contains both Co^{III}(salen)(OTf) and Co^{II}(salen$^{\bullet+}$)(OTf) character, there are four possible origins for the NIR absorptions: a ligand-to-metal charge transfer in Co^{III}(salen)-(OTf), a metal-to-ligand charge transfer in Co^{II}(salen$^{\bullet+}$)(OTf), a ligand-to-ligand charge transfer in Co^{II}(salen$^{\bullet+}$)(OTf), and an intraligand π-to-π^* transition of a phenoxyl radical. Among these possibilities, the metal-to-ligand charge transfer in Co^{II}(salen$^{\bullet+}$)(OTf) would be ruled out because the NIR absorption is shifted to a higher energy upon exchange of the MeO substituent to the *t*-Bu and Cl substituents on the salen

dx.doi.org/10.1021/ic302677f | *Inorg. Chem.* 2013, 52, 3908−3919

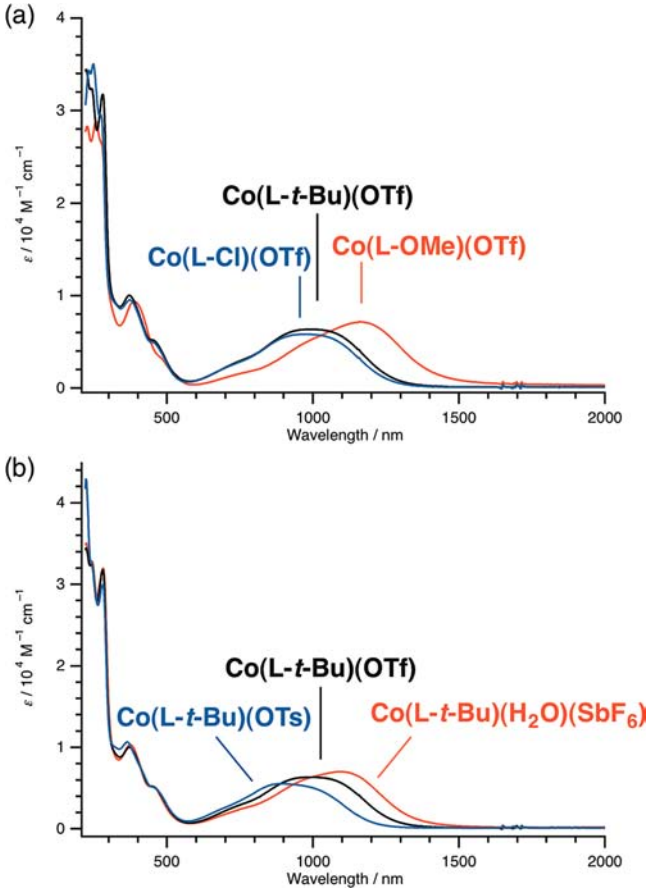

Figure 7. (a) Absorption spectra of Co(L-OMe)(OTf) (red line), Co(L-*t*-Bu)(OTf) (black line), and Co(L-Cl)(OTf) (blue line) in CH_2Cl_2 at 298 K (0.5 mM, l = 0.1 cm). (b) Absorption spectra of Co(L-*t*-Bu)(H_2O)(SbF_6) (red line) and Co(L-*t*-Bu)(OTs) (blue line), in comparison with Co(L-*t*-Bu)(OTf) (black line) in CH_2Cl_2 at 298 K (0.5 mM, l = 0.1 cm).

ligand (Figure 7a), which is the opposite of what is expected for this transition.

We then investigated axial-ligand effects. As shown in Figure 7b, the NIR absorption is dependent on the axial ligands, and thus the assignment as the intraligand π-to-π^* transition of a phenoxyl radical could be ruled out. The NIR absorption is shifted to lower wavelength in the order $SbF_6^- > TfO^- > TsO^-$. This order is exactly in parallel with the increasing order of the binding affinity to the cobalt center, as indicated by the magnitude of paramagnetic shifts (Table 4). Thus, absorption shifts by axial ligands and substituents on the salen ligand in Figure 7 are most consistent with the assignment as the ligand-to-metal charge-transfer transition from the salen ligand to the cobalt ion in the Co^{III}(salen) electronic structure.

We also measured absorption spectra of unsymmetrical Co(L-OMe/*t*-Bu)(OTf) and Co(L-OMe/Cl)(OTf) (Figure 8). The NIR absorption in Co(L-OMe)(OTf) is shifted to lower energy in Co(L-OMe/*t*-Bu)(OTf). The NIR absorption in Co(L-OMe/Cl)(OTf) is split into two bands at 1000 and 1200 nm, which are assigned as arising from the Cl−phenolate and MeO−phenolate moieties, respectively. These observations are again in agreement with the assignment of the NIR absorptions as the ligand-to-metal charge-transfer transition in the Co^{III}(salen) electronic structure. Upon cooling of the solution, the absorption around 1200 nm is significantly increased

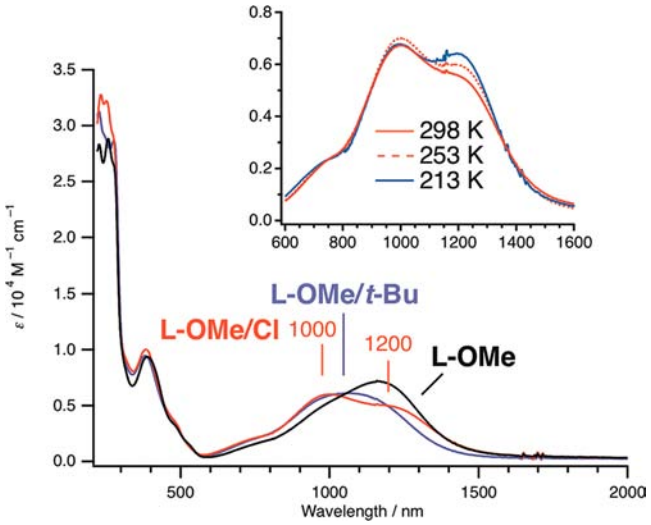

Figure 8. Absorption spectra of Co(L-OMe)(OTf) (black line), Co(L-OMe/*t*-Bu)(OTf) (purple line), and Co(L-OMe/Cl)(OTf) (red line) at 298 K (0.5 mM, l = 0.1 cm). Inset: Temperature dependence of the absorptions at 1000 and 1200 nm in Co(L-OMe/Cl)(OTf) in the range from 298 to 213 K.

compared with the absorption at 1000 nm for unsymmetrical Co(L-OMe/Cl)(OTf) (inset in Figure 8), although the NIR absorption for symmetrical Co(L-OMe)(OTf) is evenly increased (Figure S25, SI). To account for this anomalous temperature dependence, we postulated that the ligand-to-ligand charge-transfer transition in the Co^{II}(salen$^{\bullet+}$) electronic structure might be overlapped with the ligand-to-metal charge-transfer transition in the Co^{III}(salen) electronic structure. In the case of unsymmetrical Co(L-OMe/Cl)(OTf), temperature-dependent spectroscopic changes arising from the equilibrium between Co^{II}(L-OMe$^{\bullet+}$/Cl)(OTf) and Co^{II}(L-OMe/Cl$^{\bullet+}$)-(OTf) (Scheme 1) might be overlapped with other temperature-dependent spectroscopic changes from the equilibrium between Co^{III}(salen)(OTf) and Co^{II}(salen$^{\bullet+}$)(OTf), resulting in a seemingly anomalous temperature dependence.

Electronic Structure of the Co(salen)(OTf) Complex. The present structural and spectroscopic results reveal that the electronic structure of Co(salen)(OTf) contains both Co^{III}(salen)(OTf) and Co^{II}(salen$^{\bullet+}$)(OTf) character (Figure 9). As indicated by magnetic susceptibility measurements, both Co^{III}(salen)(OTf) and Co^{II}(salen$^{\bullet+}$)(OTf) belong to the S = 1 spin system. To account for the S = 1 spin system, the Co^{II}(salen$^{\bullet+}$)(OTf) complex bears the cobalt(II) center with

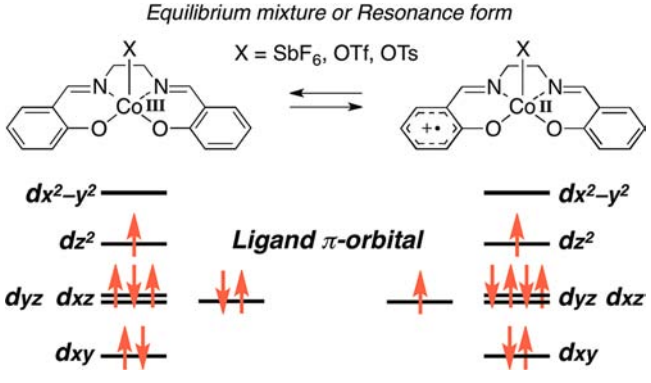

Figure 9. Proposed electronic structure of Co(salen)(X).

dx.doi.org/10.1021/ic302677f | Inorg. Chem. 2013, 52, 3908−3919

one unpaired electron in the d_{z^2} orbital, which has negligibly small antiferromagnetic coupling with the salen ligand-radical spin because of orbital symmetry. This electronic structure is also consistent with the ^{1}H NMR signal for the MeO group that shows a significant downfield shift, as a consequence of the parallel spin on the salen ligand. The electronic configuration of cobalt(II) is altered from the $(d\pi)^1$ ground state in Co^{II}(salen) to the $(d_{z^2})^1$ ground state in $Co^{II}(salen^{\bullet+})(OTf)$, probably because of coordination of a OTf^- axial ligand. The same holds true for the d-orbital energy levels in $S = 1$ Co^{III}(salen)(OTf), which bears unpaired electrons in the d_{z^2} and $d\pi$ (d_{yz} or d_{xz}) orbitals (Figure 9). From the present experimental results, it is not necessarily clear whether Co^{III}(salen)(OTf) and $Co^{II}(salen^{\bullet+})(OTf)$ might be an equilibrium mixture or a resonance form.

There have been several previous examples that resemble the present system. The Cu(L-*t*-Bu)(SbF_6) complex in the formal oxidation state of III+ shows temperature-dependent spectroscopic changes,[11c] which were assigned as thermally driven valence tautomerism between Cu^{III}(L-*t*-Bu) and Cu^{II}(L-*t*-$Bu^{\bullet+}$), as originally reported for Pierpont's complexes of catecholate and semiquinonate ligands.[18] In contrast, Wieghardt et al. reported an experimental and theoretical study on monoanionic benzene-1,2-dithiolato-, *o*-phenylenediamine-, and (*o*-aminophenol)cobalt complexes in the formal oxidation state of III+.[19] They proposed a resonance electronic structure between cobalt(III) and cobalt(II) ligand-radical species on the basis of theoretical calculations, which show that the Co 3d orbitals are placed at comparable energy with the ligand-based orbitals.

CONCLUSION

We herein investigate the molecular and electronic structures of the Co(salen)(X) catalyst (X = TsO^-, SbF_6^-, and TfO^-). The experimental results establish that the electronic structure of the Co(salen)(X) catalyst contains both Co^{III}(salen)(X) and $Co^{II}(salen^{\bullet+})(X)$ character, in contrast to the conventional assignment as a cobalt(III) complex. Such a unique electronic structure of Co(salen)(X) is distinct from Cr^{III}-, Mn^{III}-, and Fe^{III}(salen)(X) complexes.

EXPERIMENTAL SECTION

Instrumentation. Absorption spectra were recorded on a UV-3150 UV−vis−NIR spectrophotometer (Shimazdu) equipped with a USP-203 low-temperature chamber (UNISOKU), using a quartz cell (l = 0.1 cm). Absorption spectra in the solid state are measured for transparent stains on a quartz cell (l = 1 cm) that are prepared by evaporating the dilute solution of the samples and then drying in vacuo at 100 °C for 2 h. EPR spectra were recorded for 50 μL of the 2 mM frozen 30% toluene−CH_2Cl_2 solution at 4 K in a quartz tube (o.d. = 5 mm) on an E500 continuous-wave X-band spectrometer (Bruker) with an ESR910 helium-flow cryostat (Oxford Instruments). Cyclic voltammograms were measured with an ALS612A electrochemical analyzer (BAS). A saturated calomel reference electrode, a glassy carbon working electrode, and a platinum wire counter electrode were utilized. Measurements were carried out for the 1 mM solution in dehydrated CH_2Cl_2 containing 0.1 M Bu_4NOTf at a scan rate of 50 mV s^{-1} at 233 K under an argon atmosphere. The E values were referenced to the $E_{1/2}$ value of ferrocene, which was measured under identical conditions. Solid-state magnetic susceptibility measurements were carried out using a MPMS-7 SQUID susceptometer (Quantum Design) operating in the temperature range 2−320 K. Well-ground polycrystalline samples were wrapped in a plastic sheet and were loaded into the sample folder (a drinking straw). The susceptibility of the plastic sheet and the sample folder was measured in the same temperature range and field, to provide an accurate correction for its contribution to the total magnetic susceptibility. Diamagnetic corrections were estimated from Pascal constants. The simulations of μ_{eff} versus T plots were done by *julX* written by E. Bill. For details on *julX*, see http://ewww.mpi-muelheim.mpg.de/bac/logins/bill/julX_en.php. 500 MHz NMR spectra were measured in a borosilicate glass tube (o.d. = 5 mm) on a LA-500 spectrometer (JEOL). ^{1}H NMR chemical shifts in CD_2Cl_2 were referenced to $CHDCl_2$ (5.32 ppm). Electrospray ionization mass spectrometry (ESI-MS) spectra were obtained with a LCT time-of-flight mass spectrometer equipped with an ESI interface (Micromass). Elemental analyses were conducted on a CHN corder MT-6 (Yanaco). Co L-edge X-ray absorption spectra were collected at BL2A of the Ultraviolet Synchrotron Orbital Radiation Facility (UVSOR) at the Institute for Molecular Science. Finely ground solid samples were loaded into the sample cell using double-sided adhesive conductive graphite tape (Nisshin EM Corp.). The measurements were carried out at room temperature in the vacuum chamber at a pressure of 5×10^{-4} Torr or lower. For each sample, five scans were collected.

X-ray Crystallography. Measurements were made on a Rigaku/MSC Mercury CCD diffractometer equipped with graphite-monochromated Mo Kα radiation (λ = 0.71070 Å). Data were collected at 93 K under a cold nitrogen stream. All crystals were mounted on a glass fiber using epoxy glue. The images were processed with the *CrystalClear* program (version 1.3.6).[20] The structure was solved by direct methods using *SIR2004*[21] and refined by full-matrix least-squares procedures on F^2 using *SHELXL-97*,[22] on the *CrystalStructure* software package (version 4.0).[23] Anisotropic refinement was applied to all non-hydrogen atoms. Hydrogen atoms were placed at calculated positions and refined with isotropic parameters. The Flack parameters[24] were calculated to confirm the absolute configuration. The thermal ellipsoid plot was generated using *ORTEP-3* for Windows.[25]

Materials. The L-OMe, L-Cl, L-OMe/*t*-Bu, and L-OMe/Cl ligands (Chart 1) as well as the L-*t*-Bu-d_2 ligand (Chart S1, SI) were prepared according to the previously described method.[9f] The preparation of the L-*t*-Bu-d_4 ligand (Chart S1, SI) was reported previously.[9d] The preparation of Ni^{II}(salen) and Mn^{III}(salen)(OTf) complexes was reported elsewhere.[9f] Dehydrated solvents were purchased from Kanto or Wako and were utilized as received. CD_2Cl_2 was purchased from Acros and was passed though aluminum oxide (basic, Brockmann I, activated, standard grade from Aldrich) just prior to use. Cobalt(II) acetate tetrahydrate and trifluoromethanesulfonic acid (purity 98%) were purchased from Nacalai and were utilized as received. (*R*,*R*)-*N*,*N*′-Bis(3,5-di-*tert*-butylsalicylidene)-1,2-cyclohexanediamine (L-*t*-Bu) was purchased from Aldrich.

Synthesis of Co^{II}(L-OMe). The Co^{II}(salen) complexes were prepared according to the same procedure as that reported for the synthesis of Co^{II}(L-*t*-Bu) by Leung et al.[26] The solution of L-OMe (402 mg, 0.81 mmol) in toluene (5 mL) was heated at 100 °C. After dissolution, the solution of 1 equiv of $Co(OAc)_2(H_2O)_4$ (202 mg, 0.81 mmol) in ethanol (20 mL) was added. The mixture was heated at 100 °C for 5 min, and then the resulting solution was kept at 0 °C in an ice bath, affording a precipitate. The precipitate was collected and washed with ethanol to give Co^{II}(L-OMe) (220 mg, 0.40 mmol, 49%) as a purple solid, after drying in vacuo at 100 °C for 12 h. Anal. Calcd for $C_{30}H_{40}CoN_2O_4$: C, 65.32; H, 7.31; N, 5.08. Found: C, 65.26; H, 7.41; N, 5.11.

Synthesis of Co^{II}(L-*t*-Bu). The synthesis and characterization of this compound was previously reported by Leung et al.[26] The solution of L-*t*-Bu (2.00 g, 3.66 mmol) in toluene (30 mL) was heated at 100 °C. After dissolution, the solution of 1 equiv of $Co(OAc)_2(H_2O)_4$ (912 mg, 3.66 mmol) in ethanol (50 mL) was added. The mixture was heated at 100 °C for 5 min, and then the resulting solution was kept at 0 °C in an ice bath, affording a precipitate. The precipitate was collected and washed with ethanol to give Co^{II}(L-*t*-Bu) (1.65 g, 2.73 mmol, 75%) as an orange solid, after drying in vacuo at 100 °C for 12 h. Co^{II}(L-*t*-Bu-d_2) and Co^{II}(L-*t*-Bu-d_4) were synthesized in exactly the same manner.

dx.doi.org/10.1021/ic302677f | *Inorg. Chem.* 2013, 52, 3908−3919

Synthesis of Co^{II}(L-Cl). The solution of L-Cl (400 mg, 0.79 mmol) in toluene (5 mL) was heated at 100 °C. After dissolution, the solution of 1 equiv of $Co(OAc)_2(H_2O)_4$ (198 mg, 0.79 mmol) in ethanol (20 mL) was added. The mixture was heated at 100 °C for 5 min, and then the resulting solution was kept at 0 °C in an ice bath, affording a precipitate. The precipitate was collected and washed with ethanol to give Co^{II}(L-Cl) (413 mg, 0.74 mmol, 93%) as a red solid, after drying in vacuo at 100 °C for 12 h. Anal. Calcd for $C_{28}H_{34}Cl_2CoN_2O_2$: C, 60.01; H, 6.12; N, 5.00. Found: C, 59.90; H, 6.24; N, 4.99.

Synthesis of Co(L-OMe)(OTf). The solution of $Co(OAc)_2(H_2O)_4$ (201 mg, 0.81 mmol) in CH_3OH (5 mL) was added to the solution of L-OMe (200 mg, 0.40 mmol) in CH_2Cl_2 (5 mL) at room temperature. The resulting solution was stirred at room temperature for 5 h. Then, the solvent was removed by evaporation under reduced pressure. After drying in vacuo, the residue was dissolved in CH_2Cl_2 (15 mL), and an aqueous trifluoromethanesulfonic acid solution (0.5 M, 15 mL) was added. The resulting biphasic solution was vigorously stirred at room temperature for 10 h. After the addition of CH_3OH (5 mL), the organic phase was washed with an aqueous trifluoromethanesulfonic acid solution (0.5 M, 20 mL × 3). The solvent was removed by evaporation under reduced pressure. The residue was then dissolved in CH_2Cl_2–CH_3OH (10:1, 3 mL), and the resulting solution was passed through a membrane filter (Millex-FG, pore size 0.20 μm, diameter 25 mm, Millipore). The addition of pentane afforded Co(L-OMe)(OTf) (199 mg, 0.28 mmol, 70%) as a brown solid, after drying in vacuo at 100 °C for 12 h. Anal. Calcd for $C_{31}H_{40}CoF_3N_2O_7S(H_2O)_{0.2}$: C, 52.87; H, 5.78; N, 3.98. Found: C, 52.89; H, 5.78; N, 4.06.

Synthesis of Co(L-*t*-Bu)(OTf). The solution of $Co(OAc)_2(H_2O)_4$ (1.38 g, 5.54 mmol) in CH_3OH (30 mL) was added to the solution of L-*t*-Bu (1.51 g, 2.76 mmol) in CH_2Cl_2 (30 mL) at room temperature. The resulting solution was stirred at room temperature for 5 h. Then, the solvent was removed by evaporation under reduced pressure. After drying in vacuo, the residue was dissolved in CH_2Cl_2 (40 mL), and an aqueous trifluoromethanesulfonic acid solution (0.5 M, 20 mL) was added. The resulting biphasic solution was vigorously stirred at room temperature for 10 h. The organic phase was washed with an aqueous trifluoromethanesulfonic acid solution (0.5 M, 50 mL × 3). The solvent was removed by evaporation under reduced pressure. The residue was then dissolved in CH_2Cl_2 (10 mL), and the resulting solution was passed through a membrane filter (Millex-FG, pore size 0.20 μm, diameter 25 mm, Millipore). The addition of pentane afforded Co(L-*t*-Bu)(OTf) (1.94 g, 2.57 mmol, 93%) as a green solid, after drying in vacuo at 100 °C for 12 h. Anal. Calcd for $C_{37}H_{52}CoF_3N_2O_5S(H_2O)_{0.1}$: C, 58.89; H, 6.97; N, 3.71. Found: C, 58.91; H, 6.97; N, 3.72. Co(L-*t*-Bu-d_2)(OTf) and Co(L-*t*-Bu-d_4)(OTf) were synthesized in exactly the same manner.

Synthesis of Co(L-Cl)(OTf). The solution of $Co(OAc)_2(H_2O)_4$ (396 mg, 1.59 mmol) in CH_3OH (10 mL) was added to the solution of L-Cl (400 mg, 0.79 mmol) in CH_2Cl_2 (10 mL) at room temperature. The resulting solution was stirred at room temperature for 5 h. Then, the solvent was removed by evaporation under reduced pressure. After drying in vacuo, the residue was dissolved in CH_2Cl_2 (20 mL), and an aqueous trifluoromethanesulfonic acid solution (0.5 M, 15 mL) was added. The resulting biphasic solution was vigorously stirred at room temperature for 10 h. After the addition of CH_3OH (5 mL), the organic phase was washed with an aqueous trifluoromethanesulfonic acid solution (0.5 M, 20 mL × 3). The solvent was removed by evaporation under reduced pressure. The residue was then dissolved in CH_2Cl_2–CH_3OH (10:1, 3 mL), and the resulting solution was passed through a membrane filter (Millex-FG, pore size 0.20 μm, diameter 25 mm, Millipore). The addition of pentane afforded Co(L-Cl)(OTf) (535 mg, 0.72 mmol, 91%) as a green solid, after drying in vacuo at 100 °C for 12 h. Anal. Calcd for $C_{29}H_{34}Cl_2CoF_3N_2O_5S(H_2O)_{1.6}$: C, 47.18; H, 5.08; N, 3.79. Found: C, 47.19; H, 5.03; N, 3.83.

Synthesis of Co(L-OMe/*t*-Bu)(OTf). The solution of $Co(OAc)_2(H_2O)_4$ (191 mg, 0.77 mmol) in CH_3OH (5 mL) was added to the solution of L-OMe/*t*-Bu (200 mg, 0.38 mmol) in CH_2Cl_2 (5 mL) at room temperature. The resulting solution was stirred at room temperature for 5 h. Then, the solvent was removed by evaporation under reduced pressure. After drying in vacuo, the residue was dissolved in CH_2Cl_2 (15 mL), and an aqueous trifluoromethanesulfonic acid solution (0.5 M, 15 mL) was added. The resulting biphasic solution was vigorously stirred at room temperature for 10 h. After the addition of CH_3OH (5 mL), the organic phase was washed with an aqueous trifluoromethanesulfonic acid solution (0.5 M, 20 mL × 3). The solvent was removed by evaporation under reduced pressure. The residue was then dissolved in CH_2Cl_2–CH_3OH (10:1, 3 mL), and the resulting solution was passed through a membrane filter (Millex-FG, pore size 0.20 μm, diameter 25 mm, Millipore). The addition of pentane afforded Co(L-OMe/*t*-Bu)(OTf) (264 mg, 0.36 mmol, 95%) as a green solid, after drying in vacuo at 100 °C for 12 h. The ESI-MS spectrum (Figure S26a, SI) shows that the unsymmetrical complex is exclusively formed without formation of the symmetrical complexes as a result of isomerization during the synthesis. Anal. Calcd for $C_{34}H_{46}CoF_3N_2O_6S(H_2O)_{0.1}$: C, 56.05; H, 6.39; N, 3.85. Found: C, 55.99; H, 6.47; N, 3.79.

Synthesis of Co(L-OMe/Cl)(OTf). The solution of $Co(OAc)_2(H_2O)_4$ (200 mg, 0.80 mmol) in CH_3OH (5 mL) was added to the solution of L-OMe/Cl (200 mg, 0.40 mmol) in CH_2Cl_2 (5 mL) at room temperature. The resulting solution was stirred at room temperature for 5 h. Then, the solvent was removed by evaporation under reduced pressure. After drying in vacuo, the residue was dissolved in CH_2Cl_2 (15 mL), and an aqueous trifluoromethanesulfonic acid solution (0.5 M, 15 mL) was added. The resulting biphasic solution was vigorously stirred at room temperature for 10 h. After the addition of CH_3OH (5 mL), the organic phase was washed with an aqueous trifluoromethanesulfonic acid solution (0.5 M, 20 mL × 3). The solvent was removed by evaporation under reduced pressure. The residue was then dissolved in CH_2Cl_2–CH_3OH (10:1, 3 mL), and the resulting solution was passed through a membrane filter (Millex-FG, pore size 0.20 μm, diameter 25 mm, Millipore). The addition of pentane afforded Co(L-OMe/Cl)(OTf) (244 mg, 0.34 mmol, 86%) as a light-green solid, after drying in vacuo at 100 °C for 12 h. The ESI-MS spectrum (Figure S26b, SI) shows that the unsymmetrical complex is exclusively formed without formation of the symmetrical complexes as a result of isomerization during the synthesis. Anal. Calcd for $C_{30}H_{37}ClCoF_3N_2O_6S(H_2O)_{0.3}$: C, 50.72; H, 5.33; N, 3.94. Found: C, 50.74; H, 5.27; N, 3.96.

Synthesis of Co(L-*t*-Bu)(SbF_6). The solution of Co^{II}(L-*t*-Bu) (100 mg, 0.17 mmol) in CH_2Cl_2 (4 mL) was added dropwise to the solution of 1 equiv of $AgSbF_6$ (56.9 mg, 0.17 mmol) in CH_2Cl_2 (3 mL) at room temperature. The resulting solution was stirred for 5 min and was then passed through a membrane filter (Millex-FG, pore size 0.20 μm, diameter 25 mm, Millipore). The addition of pentane afforded Co(L-*t*-Bu)(SbF_6) (113 mg, 0.13 mmol, 75%) as a light-green solid, after drying in vacuo at 100 °C for 12 h. Anal. Calcd for $C_{36}H_{52}CoF_6N_2O_2Sb(H_2O)_{2.4}$: C, 48.98; H, 6.49; N, 3.17. Found: C, 48.92; H, 6.28; N, 3.21.

Synthesis of Co(L-*t*-Bu)(OTs). The solution of $Co(OAc)_2(H_2O)_4$ (911 mg, 3.66 mmol) in CH_3OH (25 mL) was added to the solution of L-*t*-Bu (1.00 g, 1.83 mmol) in CH_2Cl_2 (25 mL) at room temperature. The resulting solution was stirred at room temperature for 5 h. Then, the solvent was removed by evaporation under reduced pressure. After drying in vacuo, the residue was dissolved in CH_2Cl_2 (30 mL), and an aqueous *p*-toluenesulfonic acid solution (0.5 M, 20 mL) was added. The resulting biphasic solution was vigorously stirred at room temperature for 10 h. The organic phase was washed with an aqueous *p*-toluenesulfonic acid solution (0.5 M, 50 mL × 3). The solvent was removed by evaporation under reduced pressure. The residue was washed thoroughly with water and was then dried in vacuo. The residue was dissolved in CH_2Cl_2 (10 mL), and the resulting solution was passed through a membrane filter (Millex-FG, pore size 0.20 μm, diameter 25 mm, Millipore). The addition of pentane afforded Co(L-*t*-Bu)(OTs) (1.24 g, 1.56 mmol, 85%) as a light-green solid, after drying in vacuo at 100 °C for 12 h. Anal. Calcd for $C_{43}H_{59}CoN_2O_5S{\cdot}H_2O$: C, 65.13; H, 7.75; N, 3.53. Found: C, 65.20; H, 7.68; N, 3.55.

dx.doi.org/10.1021/ic302677f | *Inorg. Chem.* 2013, 52, 3908–3919

■ ASSOCIATED CONTENT

Supporting Information

X-ray crystallographic data in CIF format, Figures S1−S26, and Table S1. This material is available free of charge via the Internet at http://pubs.acs.org.

■ AUTHOR INFORMATION

Corresponding Author

*E-mail: hiro@ims.ac.jp.

Notes

The authors declare no competing financial interest.

■ ACKNOWLEDGMENTS

We thank Prof. Eiji Shigemasa and Naonori Kondo (UVSOR, IMS) for assistance in the measurement of Co L-edge X-ray absorption spectra. We thank Seiji Makita (IMS) for elemental analysis. This work was supported by grants from the Japan Society for the Promotion of Science (Grant-in-Aid for Scientific Research; Grants 22350030 and 23550086).

■ REFERENCES

(1) Jacobsen, E. N. *Acc. Chem. Res.* **2000**, *33*, 421−431.

(2) (a) Tokunaga, M.; Larrow, J. F.; Kakiuchi, F.; Jacobsen, E. N. *Science* **1997**, *277*, 936−938. (b) Schaus, S. E.; Brandes, B. D.; Larrow, J. F.; Tokunaga, M.; Hansen, K. B.; Gould, A. E.; Furrow, M. E.; Jacobsen, E. N. *J. Am. Chem. Soc.* **2002**, *124*, 1307−1315. (c) Welbes, L. L.; Scarrow, R. C.; Borovik, A. S. *Chem. Commun.* **2004**, 2544−2545. (d) Rossbach, B. M.; Leopold, K.; Weberskirch, R. *Angew. Chem., Int. Ed.* **2006**, *45*, 1309−1312. (e) Dey, S.; Powell, D. R.; Hu, C.; Berkowitz, D. B. *Angew. Chem., Int. Ed.* **2007**, *46*, 7010−7014. (f) Zheng, X.; Jones, C. W.; Weck, M. *J. Am. Chem. Soc.* **2007**, *129*, 1105−1112.

(3) (a) Ready, J. M.; Jacobsen, E. N. *J. Am. Chem. Soc.* **1999**, *121*, 6086−6087. (b) Huang, Y.; Iwama, T.; Rawal, V. H. *J. Am. Chem. Soc.* **2002**, *124*, 5950−5951. (c) Kang, S. H.; Lee, S. B.; Park, C. M. *J. Am. Chem. Soc.* **2003**, *125*, 15748−15749. (d) Shen, Y.-M.; Duan, W.-L.; Shi, M. *J. Org. Chem.* **2003**, *68*, 1559−1562. (e) Kim, S. K.; Jacobsen, E. N. *Angew. Chem., Int. Ed.* **2004**, *43*, 3952−3954. (f) Lu, X.-B.; Liang, B.; Zhang, Y.-J.; Tian, Y.-Z.; Wang, Y.-M.; Bai, C.-X.; Wang, H.; Zhang, R. *J. Am. Chem. Soc.* **2004**, *126*, 3732−3733. (g) Paddock, R. L.; Nguyen, S. T. *Chem. Commun.* **2004**, 1622−1623. (h) Kim, H.-J.; Kim, W.; Lough, A. J.; Kim, B. M.; Chin, J. *J. Am. Chem. Soc.* **2005**, *127*, 16776−16777. (i) Peretti, K. L.; Ajiro, H.; Cohen, C. T.; Lobkovsky, E. B.; Coates, G. W. *J. Am. Chem. Soc.* **2005**, *127*, 11566−11567. (j) Hutson, G. E.; Dave, A. H.; Rawal, V. H. *Org. Lett.* **2007**, *9*, 3869−3872. (k) Hirahata, W.; Thomas, R. M.; Lobkovsky, E. B.; Coates, G. W. *J. Am. Chem. Soc.* **2008**, *130*, 17658−17659. (l) Park, J.; Lang, K.; Abboud, K. A.; Hong, S. *J. Am. Chem. Soc.* **2008**, *130*, 16484−16485. (m) Loy, R. N.; Jacobsen, E. N. *J. Am. Chem. Soc.* **2009**, *131*, 2786−2787. (n) Kalow, J. A.; Doyle, A. G. *J. Am. Chem. Soc.* **2010**, *132*, 3268−3269. (o) Thomas, R. M.; Widger, P. C. B.; Ahmed, S. M.; Jeske, R. C.; Hirahata, W.; Lobkovsky, E. B.; Coates, G. W. *J. Am. Chem. Soc.* **2010**, *132*, 16520−16525.

(4) Darensbourg, D. J. *Chem. Rev.* **2007**, *107*, 2388−2410.

(5) (a) Qin, Z.; Thomas, C. M.; Lee, S.; Coates, G. W. *Angew. Chem., Int. Ed.* **2003**, *42*, 5484−5487. (b) Lu, X.-B.; Wang, Y. *Angew. Chem., Int. Ed.* **2004**, *43*, 3574−3577. (c) Cohen, C. T.; Chu, T.; Coates, G. W. *J. Am. Chem. Soc.* **2005**, *127*, 10869−10878. (d) Lu, X.-B.; Shi, L.; Wang, Y.-M.; Zhang, R.; Zhang, Y.-J.; Peng, X.-J.; Zhang, Z.-C.; Li, B. *J. Am. Chem. Soc.* **2006**, *128*, 1664−1674. (e) Nakano, K.; Kamada, T.; Nozaki, K. *Angew. Chem., Int. Ed.* **2006**, *45*, 7274−7277. (f) Noh, E. K.; Na, S. J.; S, S.; Kim, S.-W.; Lee, B. Y. *J. Am. Chem. Soc.* **2007**, *129*, 8082−8083. (g) S, S.; Min, J. K.; Seong, J. E.; Na, S. J.; Lee, B. Y. *Angew. Chem., Int. Ed.* **2008**, *47*, 7306−7309. (h) Wu, G.-P.; Wei, S.-H.; Ren, W.-M.; Lu, X.-B.; Xu, T.-Q.; Darensbourg, D. J. *J. Am. Chem. Soc.* **2011**, *133*, 15191−15199. (i) Wu, G.-P.; Ren, W.-M.; Luo, Y.; Li, B.; Zhang, W.-Z.; Lu, X.-B. *J. Am. Chem. Soc.* **2012**, *134*, 5682−5688.

(6) (a) Nishikawa, H.; Yamada, S. *Bull. Chem. Soc. Jpn.* **1964**, *37*, 8−12. (b) Hoffman, B. M.; Basolo, F.; Diemente, D. L. *J. Am. Chem. Soc.* **1973**, *95*, 6497−6498. (c) Murray, K. S.; Sheahan, R. M. *Chem. Phys. Lett.* **1973**, *22*, 406−410. (d) Burness, J. H.; Dillard, J. G.; Taylor, L. T. *J. Am. Chem. Soc.* **1975**, *97*, 6080−6088. (e) Migita, K.; Iwaizumi, M.; Isobe, T. *J. Am. Chem. Soc.* **1975**, *97*, 4228−4232. (f) Hitchman, M. A. *Inorg. Chem.* **1977**, *16*, 1985−1993. (g) Srivanavit, C.; Brown, D. G. *J. Am. Chem. Soc.* **1978**, *100*, 5777−5783.

(7) (a) Nielsen, L. P.; Stevenson, C. P.; Blackmond, D. G.; Jacobsen, E. N. *J. Am. Chem. Soc.* **2004**, *126*, 1360−1362. (b) Cohen, C. T.; Thomas, C. M.; Peretti, K. L.; Lobkovsky, E. B.; Coates, G. W. *Dalton Trans.* **2006**, 237−249. (c) Jain, S.; Zheng, X.; Jones, C. W.; Weck, M.; Davis, R. J. *Inorg. Chem.* **2007**, *46*, 8887−8896. (d) Ajiro, H.; Peretti, K. L.; Lobkovsky, E. B.; Coates, G. W. *Dalton Trans.* **2009**, 8828−8830. (e) Kemper, S.; Hrobárik, P.; Kaupp, M.; Schlörer, N. E. *J. Am. Chem. Soc.* **2009**, *131*, 4172−4173. (f) Na, S. J.; S, S.; Cyriac, A.; Kim, B. E.; Yoo, J.; Kang, Y. K.; Han, S. J.; Lee, C.; Lee, B. Y. *Inorg. Chem.* **2009**, *48*, 10455−10465. (g) Ren, W.-M.; Liu, Z.-W.; Wen, Y.-Q.; Zhang, R.; Lu, X.-B. *J. Am. Chem. Soc.* **2009**, *131*, 11509−11518. (h) Vinck, E.; Murphy, D. M.; Fallis, I. A.; Strevens, R. R.; Van Doorslaer, S. *Inorg. Chem.* **2010**, *49*, 2083−2092. (i) Kalow, J. A.; Doyle, A. G. *J. Am. Chem. Soc.* **2011**, *133*, 16001−16012. (j) Cyriac, A.; Jeon, J. Y.; Varghese, J. K.; Park, J. H.; Choi, S. Y.; Chung, Y. K.; Lee, B. Y. *Dalton Trans.* **2012**, *41*, 1444−1447. (k) Vinck, E.; Carter, E.; Murphy, D. M.; Van Doorslaer, S. *Inorg. Chem.* **2012**, *51*, 8014−8024.

(8) Kochem, A.; Kanso, H.; Baptiste, B.; Arora, H.; Philouze, C.; Jarjayes, O.; Vezin, H.; Luneau, D.; Orio, M.; Thomas, F. *Inorg. Chem.* **2012**, *51*, 10557−10571.

(9) (a) Kurahashi, T.; Kobayashi, Y.; Nagatomo, S.; Tosha, T.; Kitagawa, T.; Fujii, H. *Inorg. Chem.* **2005**, *44*, 8156−8166. (b) Kurahashi, T.; Fujii, H. *Inorg. Chem.* **2008**, *47*, 7556−7567. (c) Kurahashi, T.; Kikuchi, A.; Tosha, T.; Shiro, Y.; Kitagawa, T.; Fujii, H. *Inorg. Chem.* **2008**, *47*, 1674−1686. (d) Kurahashi, T.; Hada, M.; Fujii, H. *J. Am. Chem. Soc.* **2009**, *131*, 12394−12405. (e) Kurahashi, T.; Kikuchi, A.; Shiro, Y.; Hada, M.; Fujii, H. *Inorg. Chem.* **2010**, *49*, 6664−6672. (f) Kurahashi, T.; Fujii, H. *J. Am. Chem. Soc.* **2011**, *133*, 8307−8316. (g) Kurahashi, T.; Fujii, H. *Bull. Chem. Soc. Jpn.* **2012**, *85*, 940−947. (h) Wang, C.; Kurahashi, T.; Fujii, H. *Angew. Chem., Int. Ed.* **2012**, *51*, 7809−7811.

(10) $Ni^{II}(salen^{\bullet+})$ complexes: (a) Shimazaki, Y.; Tani, F.; Fukui, K.; Naruta, Y.; Yamauchi, O. *J. Am. Chem. Soc.* **2003**, *125*, 10512−10513. (b) Rotthaus, O.; Jarjayes, O.; Thomas, F.; Philouze, C.; Perez Del Valle, C.; Saint-Aman, E.; Pierre, J.-L. *Chem.—Eur. J.* **2006**, *12*, 2293−2302. (c) Rotthaus, O.; Thomas, F.; Jarjayes, O.; Philouze, C.; Saint-Aman, E.; Pierre, J.-L. *Chem.—Eur. J.* **2006**, *12*, 6953−6962. (d) Benisvy, L.; Kannappan, R.; Song, Y.-F.; Milikisyants, S.; Huber, M.; Mutikainen, I.; Turpeinen, U.; Gamez, P.; Bernasconi, L.; Baerends, E. J.; Hartl, F.; Reedijk, J. *Eur. J. Inorg. Chem.* **2007**, 637−642. (e) Rotthaus, O.; Jarjayes, O.; Perez Del Valle, C.; Philouze, C.; Thomas, F. *Chem. Commun.* **2007**, 4462−4464. (f) Shimazaki, Y.; Yajima, T.; Tani, F.; Karasawa, S.; Fukui, K.; Naruta, Y.; Yamauchi, O. *J. Am. Chem. Soc.* **2007**, *129*, 2559−2568. (g) Storr, T.; Wasinger, E. C.; Pratt, R. C.; Stack, T. D. P. *Angew. Chem., Int. Ed.* **2007**, *46*, 5198−5201. (h) Shimazaki, Y.; Stack, T. D. P.; Storr, T. *Inorg. Chem.* **2009**, *48*, 8383−8392. (i) Kochem, A.; Orio, M.; Jarjayes, O.; Neese, F.; Thomas, F. *Chem. Commun.* **2010**, *46*, 6765−6767. (j) Storr, T.; Verma, P.; Shimazaki, Y.; Wasinger, E. C.; Stack, T. D. P. *Chem.—Eur. J.* **2010**, *16*, 8980−8983. (k) Shimazaki, Y.; Arai, N.; Dunn, T. J.; Yajima, T.; Tani, F.; Ramogida, C. F.; Storr, T. *Dalton Trans.* **2011**, *40*, 2469−2479. (l) Chiang, L.; Kochem, A.; Jarjayes, O.; Dunn, T. J.; Vezin, H.; Sakaguchi, M.; Ogura, T.; Orio, M.; Shimazaki, Y.; Thomas, F.; Storr, T. *Chem.—Eur. J.* **2012**, *18*, 14117−14127.

(11) $Cu^{II}(salen^{\bullet+})$ complexes: (a) Pratt, R. C.; Stack, T. D. P. *J. Am. Chem. Soc.* **2003**, *125*, 8716−8717. (b) Pratt, R. C.; Stack, T. D. P. *Inorg. Chem.* **2005**, *44*, 2367−2375. (c) Storr, T.; Verma, P.; Pratt, R. C.; Wasinger, E. C.; Shimazaki, Y.; Stack, T. D. P. *J. Am. Chem. Soc.* **2008**, *130*, 15448−15459. (d) Verma, P.; Pratt, R. C.; Storr, T.;

Wasinger, E. C.; Stack, T. D. P. *Proc. Natl. Acad. Sci. U.S.A.* **2011**, *108*, 18600−18605. (e) Pratt, R. C.; Lyons, C. T.; Wasinger, E. C.; Stack, T. D. P. *J. Am. Chem. Soc.* **2012**, *134*, 7367−7377.
(12) Ni^{II}- and $Cu^{II}(salen^{\bullet+})$ complexes: Orio, M.; Jarjayes, O.; Kanso, H.; Philouze, C.; Neese, F.; Thomas, F. *Angew. Chem., Int. Ed.* **2010**, *49*, 4989−4992.
(13) Hocking, R. K.; DeBeer George, S.; Raymond, K. N.; Hodgson, K. O.; Hedman, B.; Solomon, E. I. *J. Am. Chem. Soc.* **2010**, *132*, 4006−4015.
(14) (a) Kennedy, B. J.; Fallon, G. D.; Gatehouse, B. M. K. C.; Murray, K. S. *Inorg. Chem.* **1984**, *23*, 580−588. (b) Zarembowitch, J.; Kahn, O. *Inorg. Chem.* **1984**, *23*, 589−593.
(15) McConnell, H. M.; Chesnut, D. B. *J. Chem. Phys.* **1958**, *28*, 107.
(16) LaMar, G. N.; Horrocks, W. D.; Holm, R. H. *NMR of Paramagnetic Molecules*; Academic Press: New York, 1973.
(17) (a) Brede, O.; Orthner, H.; Zubarev, V.; Hermann, R. *J. Phys. Chem.* **1996**, *100*, 7097−7105. (b) Sokolowski, A.; Müller, J.; Weyhermüller, T.; Schnepf, R.; Hildebrandt, P.; Hildenbrand, K.; Bothe, E.; Wieghardt, K. *J. Am. Chem. Soc.* **1997**, *119*, 8889−8900.
(18) (a) Buchanan, R. M.; Pierpont, C. G. *J. Am. Chem. Soc.* **1980**, *102*, 4951−4957. (b) Pierpont, C. G. *Coord. Chem. Rev.* **2001**, *216*−*217*, 99−125.
(19) (a) Bill, E.; Bothe, E.; Chaudhuri, P.; Chlopek, K.; Herebian, D.; Kokatam, S.; Ray, K.; Weyhermüller, T.; Neese, F.; Wieghardt, K. *Chem.—Eur. J.* **2005**, *11*, 204−224. (b) Ray, K.; Begum, A.; Weyhermüller, T.; Piligkos, S.; van Slageren, J.; Neese, F.; Wieghardt, K. *J. Am. Chem. Soc.* **2005**, *127*, 4403−4415. (c) Ray, K.; DeBeer George, S.; Solomon, E. I.; Wieghardt, K.; Neese, F. *Chem.—Eur. J.* **2007**, *13*, 2783−2797.
(20) *CrystalClear: An Integrated Program for the Collection and Processing of Area Detector Data*, Rigaku Corp.
(21) Burla, M. C.; Caliandro, R.; Camalli, M.; Carrozzini, B.; Cascarano, G. L.; De Caro, L.; Giacovazzo, C.; Polidori, G.; Spagna, R. *J. Appl. Crystallogr.* **2005**, *38*, 381−388.
(22) Sheldrick, G. M. *Acta Crystallogr., Sect. A: Found. Crystallogr.* **2008**, *64*, 112−122.
(23) *CrystalStructure: Crystal Structure Analysis Package*, Rigaku Corp.
(24) Flack, H. D. *Acta Crystallogr., Sect. A: Found. Crystallogr.* **1983**, *39*, 876−881.
(25) Farrugia, L. J. *J. Appl. Crystallogr.* **1997**, *30*, 565−565.
(26) Leung, W.-H.; Chan, E. Y. Y.; Chow, E. K. F.; Williams, I. D.; Peng, S.-M. *J. Chem. Soc., Dalton Trans.* **1996**, 1229−1236.